CHIN. PHYS. LETT. Vol. 37, No. 10 (2020) 107101

Coupling Stacking Orders with Interlayer Magnetism in Bilayer H-VSe_2

Aolin Li(李奥林)[1], Wenzhe Zhou(周文哲)[1], Jiangling Pan(潘江陵)[2], Qinglin Xia(夏庆林)[2], Mengqiu Long(龙孟秋)[2,3], and Fangping Ouyang(欧阳方平)[1,2,3*]

[1]*State Key Laboratory of Powder Metallurgy, and Powder Metallurgy Research Institute, Central South University, Changsha 410083, China*

[2]*School of Physics and Electronics, and Hunan Key Laboratory for Super-Microstructure and Ultrafast Process, Central South University, Changsha 410083, China*

[3]*School of Physics and Technology, Xinjiang University, Urumqi 830046, China*

(Received 9 July 2020; accepted 8 August 2020; published online 29 September 2020)

Stacking-dependent magnetism in van der Waals materials has caught intense interests. Based on the first principle calculations, we investigate the coupling between stacking orders and interlayer magnetic orders in bilayer H-VSe_2. It is found that there are two stable stacking orders in bilayer H-VSe_2, named AB-stacking and A′B-stacking. Under standard DFT framework, the A′B-stacking prefers the interlayer AFM order and is semiconductive, whereas the AB-stacking prefers the FM order and is metallic. However, under the DFT+U framework both the stacking orders prefer the interlayer AFM order and are semiconductive. By detailedly analyzing this difference, we find that the interlayer magnetism originates from the competition between antiferromagnetic interlayer super-superexchange and ferromagnetic interlayer double exchange, in which both the interlayer Se-4p_z orbitals play a crucial role. In the DFT+U calculations, the double exchange is suppressed due to the opened bandgap, such that the interlayer magnetic orders are decoupled with the stacking orders. Based on this competition mechanism, we propose that a moderate hole doping can significantly enhance the interlayer double exchange, and can be used to switch the interlayer magnetic orders in bilayer VSe_2. This method is also applicable to a wide range of semiconductive van der Waals magnets.

PACS: 71.70.Gm, 75.30.Et, 71.15.Mb, 71.30.+h DOI: 10.1088/0256-307X/37/10/107101

The stacking-dependent properties in van der Waals (vdW) materials have caught wide attention for nanoelectronic applications. Although the interlayer coupling is weak in energy, it can cause drastic influence on the electronic properties by interlayer charge transfer,[1] wavefunction hybridization,[2] magnetic exchange,[3,4] and spin-orbit proximity,[5,6] etc. Recently, the atomically thin CrI_3 has been experimentally exfoliated and displays thickness-dependent magnetism due to the interlayer antiferromagnetic (AFM) coupling.[7] First-principles calculations have suggested that the interlayer coupling in bilayer CrI_3 can either be ferromagnetic (FM) or antiferromagnetic by switching the stacking orders.[3,4] This has been confirmed by recent experiments in which hydrostatic pressures were used to control the stacking orders and interlayer magnetic orders.[8,9] Despite the fascinating interlayer magnetism in CrI_3, the low Curie temperature (∼45 K for the monolayer[7]) greatly restrict its application in spintronic. Seeking 2D materials with both room-temperature and stacking-dependent magnetism is of important value, but remains great challenging.

Besides CrI_3, there are some other two-dimensional (2D) magnets that have been fabricated in laboratories, including $Cr_2Ge_2Te_6$,[10] Fe_3GeTe_2,[11] VSe_2,[12] $MnSe_2$,[13] etc.,[14,15] while stacking-dependent magnetism has few been reported in these materials. Instead, the stacking-induced magnetism has been found in some nonmagnetic materials.[16,17] For example, in the twisted bilayer graphene,[16] bilayer silicone and germanene,[17] first-principles calculations have suggested that spontaneous magnetization can be induced by the stacking effects, but this magnetism seems not to be maintained at room temperature. Remarkably, Zhou *et al.* have reported a Bethe-Slater-Curve (BSC) like behavior in bilayer chromium dichalcogenides, in which the interlayer AFM order and FM order are preferred at shorter and longer distances, respectively.[18] Inspired by their work, we propose that the stacking-dependent magnetism may be realized in 2D magnets, as long as the interlayer distances fall into the FM and AFM regions for different stacking orders, respectively.

In this work, we choose vanadium selenide (VSe_2) to explore the stacking-dependent magnetism, because of its strong magnetism and semiconducting properties for spintronic applications. There

Supported by the National Natural Science Foundation of China (Grant No. 51272291), the Distinguished Young Scholar Foundation of Hunan Province (Grant No. 2015JJ1020), the Young Scholar Foundation of Hunan Province (Grant No. 2016JJ3142), the Central South University Research Fund for Sheng-Hua Scholars, Central South University State Key Laboratory of Powder Metallurgy, and the Fundamental Research Funds for the Central Universities of Central South University.

*Corresponding author. Email: oyfp@csu.edu.cn

© 2020 Chinese Physical Society and IOP Publishing Ltd

are two polymorphs for VSe_2, the semiconductive hexagonal (H) phase and the metallic octahedral (T) phase. The monolayer T-VSe_2 has been successfully synthesized in 2018, and its strong room-temperature ferromagnetism on van der Waals substrates is demonstrated.[12] Although atomically thin H-VSe_2 has not been synthesized in laboratory, its bulk material 3R-VSe_2 was reported very early.[19] The first principles calculation has suggested that the Curie temperature of monolayer H-VSe_2 can reach 541 K.[20] Recent studies have shown that the bilayer H-VSe_2 is of great potential in achieving all-electric valleytronics and spintronics.[21,22]

All density functional theory (DFT) calculations in this work are performed with the Vienna *ab initio* Simulation Package (VASP).[23] Generalized gradient approximation (GGA) with the PBE formalism[24] and projected augmented wave (PAW) pseudopotentials[25] are used. The cutoff energy of the plane waves is set to 500 eV, and the k-points are sampled on a $21 \times 21 \times 1$ Monkhorst–Pack grid. For the structural relaxation, the tolerance of the Hellmann–Feynman forces is set as 1 meV/Å, and for self-consistent calculations, the energy convergence criterion is set as 10^{-7} eV. A vacuum layer thicker than 10 Å along the c axis is used to screen the interaction between neighbor repeated imagines. To describe the interlayer van der Waals interactions, the DFT-D2 method is used.[26] DFTs without and with Hubbard U correction[27] for V-3d orbitals are both performed, and the difference is carefully compared. Our results suggest that Hubbard U correction only makes little effects on the structural stability and relative energies for different stacking orders, while can significantly affect the bandgap and interlayer magnetic coupling. The effect of spin-orbit coupling (SOC) is negligible for the results, thereby the DFT+SOC calculations are not considered in this work (see the Supplementary Material).

Bilayer VSe_2 is usually considered to have an AB-stacking order as 2H-MoS_2, but other stacking order may also be stable. For example, Fig. 1(a) shows three possible stacking orders with high symmetry. In the AB-stacking, the V(Se) atoms of the upper layer cover the Se (V) atoms of the nether layer. In the A′B-stacking, the V atoms of the upper layer cover the V atoms of the nether layer, while the Se atoms in different layers are staggered. In the AA′-stacking, the Se atoms in different layers are directly head-to-head whereas the V atoms are staggered.

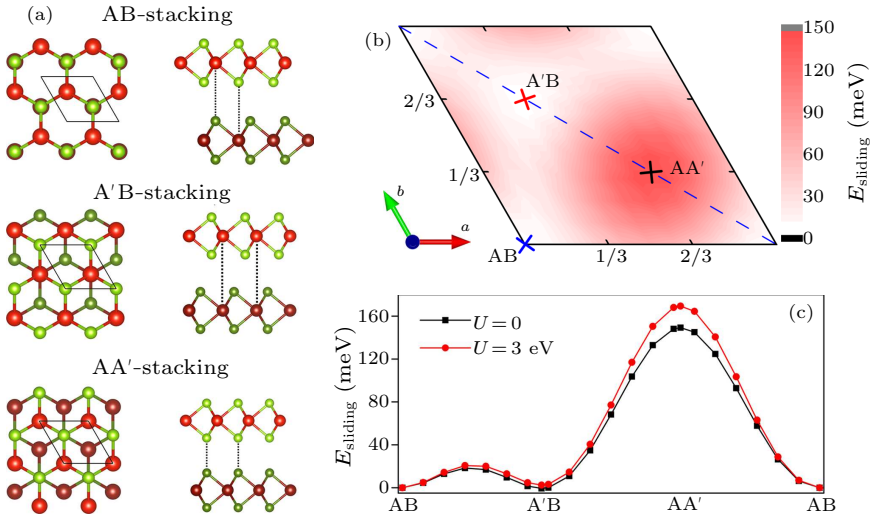

Fig. 1. (a) Three high-symmetry stacking orders in bilayer H-VSe_2. (b) The sliding energy landscape, the blue dashed line represents the high-symmetry [1$\bar{1}$0] direction. (c) The sliding energy along the high-symmetry [1$\bar{1}$0] direction.

To explore all possible stable stacking orders in bilayer H-VSe_2, we use the fully relaxed AB-stacking VSe_2 as the initial structure. When keeps the nether layer fixed, the upper layer is rigidly shifted along the (001) plane. The sliding energy $\Delta E_{\rm sliding}$ is defined as

$$\Delta E_{\rm sliding} = E_{\rm shift} - E_{\rm AB}, \tag{1}$$

where $E_{\rm AB}$ and $E_{\rm shift}$ represent the total energy of AB-stacking and the shifted configuration, respectively. The calculated sliding energy landscape is shown in Fig. 1(b), apart from the initial AB stacking, we find that the A′B stacking is also energy-favored. Both AB and A′B stackings belong to the $P\bar{3}M1$ space group and have the same crystallographic symmetries, their energy difference is within 3 meV per formula unit (f.u.). The AA′-stacking is the most unstable in energy due to strong Pauli repulsion between the head-to-head interlayer Se atoms. Figure 1(c) shows the $\Delta E_{\rm sliding}$ along the high-symmetry [1$\bar{1}$0] direction, the energy of AA′-stacking is over 130 meV/f.u. higher than the two energy-favored stacking orders. The energy barrier between the AB- and A′B-stackings is only ∼20 meV/f.u., similar to the values of bilayer CrI_3.[3,4] The Hubbard U correction is considered in

Fig. 1(c), which makes little impact on the results. The dynamical stability of AB- and A′B-stacking has been checked by the phonon spectrum (see Fig. S1 in the Supplementary Material), which agrees well with the literature.[28]

To understand the stacking effect of bilayer H-VSe_2, knowledge about the fundamental electronic nature of monolayer VSe_2 is necessary. Figure 2 shows the band structure of monolayer VSe_2 and its major orbital contributions. We are concerned with only two bands around the Fermi level (E_F), the highest-occupied valence band (marked as α-band) and the lowest-unoccupied conduction band (marked as β-band). Nominally, the V^{4+} ion has an electronic configuration $3d^1 4s^0$. When spin polarization is not considered, a single d-band will cross the E_F under the hexahedral crystal field, which makes the monolayer VSe_2 metallic and a high density of states (DOS) at the E_F (see Fig. S2 in the Supplementary Material). After spin-polarization is considered as shown in Fig. 2, the single d-band spontaneously splits into the α- and β-bands due to the Stoner instability.

Under the DFT framework, the spin splitting energy E_s between the α- and β-bands is about 1 eV at the Γ point, which opens a small indirect bandgap E_g on the value of 0.25 eV. After considering the Hubbard U correction, both the spin splitting energy and the bandgap increase with the increasing U parameter (see Fig. S3 in the Supplementary Material). From Fig. 2 we can find that the α- and β-bands are mainly contributed by V-$3d_{z^2}$ orbital around the Γ point, while the Se-$4p_z$ orbitals have only a very small contribution (∼3%). However, this small Se-$4p_z$ contribution plays a pivotal role in the band structure evolution when stacking into multilayers.

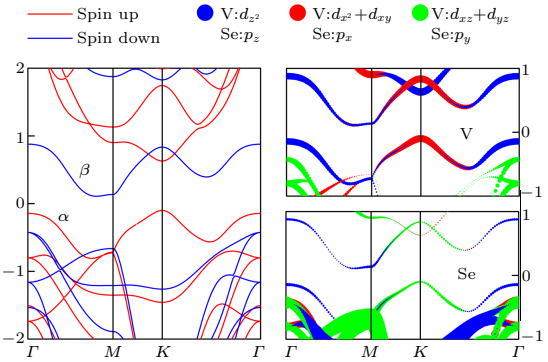

Fig. 2. The band structure of monolayer H-VSe_2 (left) and its major orbital contribution. For clarity, the projection weight of Se-4p orbitals is set as ten times the value of V-3d orbitals.

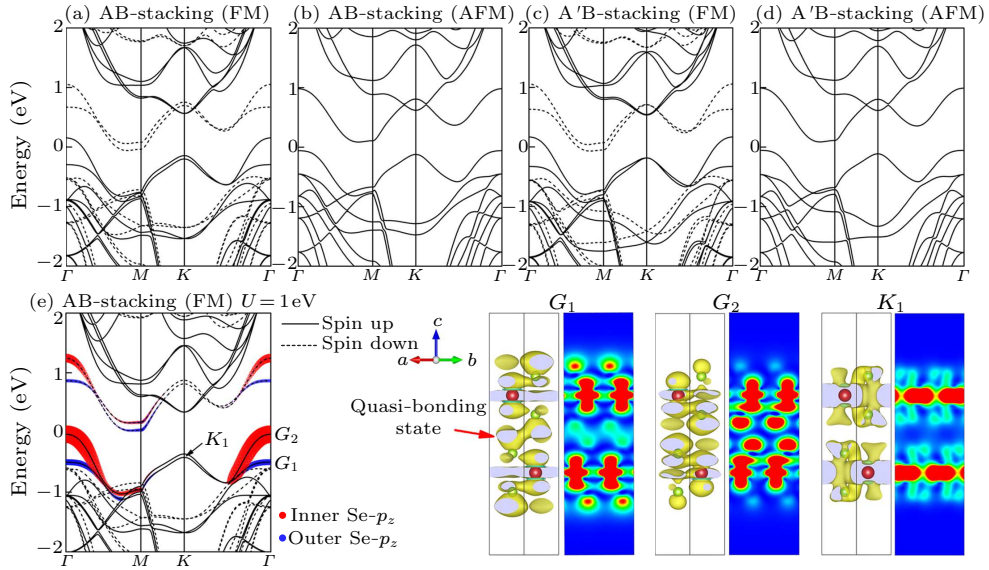

Fig. 3. (a)–(d) The band structures of bilayer H-VSe_2 with different stacking modes and magnetic orders. (e) The projected band structure for the interlayer and outerlayer Se-$4p_z$ orbitals with $U = 1$ eV. (f) The visualized wave functions for the eigenstates labeled in (e), where the contour surface is set as $5 \times 10^{-4}\, e/\text{Å}^3$.

Figures 3(a)–3(d) show the band structures of bilayer VSe_2, the difference is fractional between AB- and A′B-stacking orders, while it is obvious between the FM and interlayer AFM orders. In terms of the interlayer AFM order, both the α- and β-bands are spin-degenerate, and the bilayers remain semiconductive. In terms of the FM order, a band splitting appears in the α- and β-bands, which makes the FM bilayers change into metallic. The total energies of bilayer H-VSe_2 are listed in Table 1. We find that the AB-stacking prefers the FM order, while the A′B-stacking prefers the interlayer AFM order. This suggests that a semiconductor-to-metal transition in bilayer H-VSe_2 can be achieved by switching either the stacking orders or the interlayer magnetic orders. However, the usage of Hubbard U correction causes the bandgap not to be fully closed for the FM orders. For example, Fig. 3(e) shows that a bandgap on the value of ∼60 meV is

opened for the FM bilayer with $U = 1$ eV. However, even without the gap closing, the interlayer magnetic orders can still cause a big difference in the conductivity or carrier concentration σ. The bandgap difference ΔE_g between FM and interlayer AFM orders is about 350 meV. Using the relationship $\sigma \propto \exp(-E_g/k_B T)$, we estimate that the carrier concentration of FM orders is about 10^5 times larger than the AFM orders at room temperature.

Table 1. The total energy of bilayer VSe_2 per unit cell with reference to the FM AB-stacking and the band gaps. For the DFT+U calculations, an effective on-site U on the value of 1.0 eV is used.

		AB		A′B	
		FM	AFM	FM	AFM
DFT	Energy (meV)	0	0.3	−1.1	−1.2
	Gap (eV)	0	0.15	0	0.14
DFT+U	Energy (meV)	0	−3.3	2.1	−2.0
	Gap (eV)	0.06	0.39	0.04	0.38

From Figs. 3(a) and 3(c), we can find that the band splittings are significant around the G and M points, where the Se-p_z orbitals have a contribution to the bands (see Fig. 2), indicating that the interlayer Se-4p_z orbitals play a crucial role in the band splitting. By analyzing the eigenstates of α- and β-bands, we attribute this splitting to the interlayer covalent-like Se···Se quasi-bonding states, which is first proposed by Zhao *et al.*[2] and has been recently confirmed by experiments.[29] The Bloch states for the split α-band at the G and K points are labeled as G_1, G_2, and K_1 as shown in Fig. 3(e), and are visualized in Fig. 3(f). For the lower-energy G_1 point, the interlayer Se-4p_z orbitals in adjacent layers are hybridized with each other, corresponding to the interlayer quasi-bonding state. For the higher-energy G_2 point, the interlayer Se-4p_z orbitals are separated from each other, corresponding to the interlayer anti-bonding state. At the K_1 point, because the Se-4p_z orbital contribution is absent, the wavefunction is separated at the vdW gap and the band splitting is suppressed. For the interlayer AFM orders, the spin degeneracy is preserved by its invariance under the combination of time-reversal operation and inversion operation, such that the band splitting is suppressed.

Figure 3(e) also shows the contribution of interlayer/outerlayer Se-4p_z orbitals to the α- and β-bands. We can find that the inner Se-4p_z orbitals mainly contribute to the upper bands, while the outer Se-4p_z orbitals mainly contribute to the lower bands. In addition, our DFT calculations show that each Se ion has $\sim 0.1\mu_B$ magnetic moment antiparallel to the one of V ions ($\sim 1.1\mu_B$). The Pauli repulsion between interlayer Se ions will make the bilayers prefer to form an interlayer AFM order.

To study the relationship between stacking orders and interlayer magnetic orders, we plot the landscape of interlayer exchange energy in Fig. 4(a). The interlayer exchange energy can be defined as the energy difference between the FM order and the interlayer AFM order per unit cell:

$$J_{ex} = E(\mathrm{FM}) - E(\mathrm{AFM}), \tag{2}$$

such that a negative value means that the bilayers prefers the FM orders, while a positive value means that the bilayers prefers the interlayer AFM order.

In Fig. 4(a), the DFT results show obvious stacking-dependent magnetism in bilayer VSe_2. While the AB- and AA′-stacking prefer the FM order, the A′B-stacking prefers the interlayer AFM order. After considering the Hubbard U correction, we find that all configurations favor the interlayer AFM state, such that the stacking orders and interlayer magnetic orders are decoupled. To understand this difference, a clear picture of the interlayer magnetic exchange coupling is necessary. Although direct exchange between V ions in different layers is impossible due to the big distance, the interlayer magnetic exchange can also be established through indirect ways, such as the super-superexchange (SSE)[4] and the double exchange (DE),[30,31] which are mediated by the intermediate Se ions and conduction electrons, respectively.

We first consider the SSE mechanism that two spin-polarized electrons in different layers are coupled through a V–Se···Se–V path, in which the Se···Se represents the covalent-like quasi-bonding between interlayer Se atoms. This mechanism has successfully been used to explain the interlayer AFM order in the bilayer $CrSe_2$.[18] Considering the structural similarities of VSe_2 and $CrSe_2$, we believe that the SSE also plays an important role in bilayer VSe_2. The V 3d orbits of VSe_2 has the $t_{2g}^1 e_g^0$ occupied states under the hexahedral crystal field, containing both half-filled and empty V 3d orbitals. According to the Goodenough–Kanamori rule,[32,33] the SSE coupling can either be AFM or FM depending on the two sequential V–Se···Se bond angles. Our results suggest that there are two typical bond angles, the nearly orthogonal one ($\theta_1 \approx 93°$) and the nearly collinear one ($\theta_2 \approx 140°$), as shown in Fig. 4(c). Their combination leads to three different SSE paths, i.e., (θ_1, θ_1), (θ_1, θ_2) and (θ_2, θ_2). Notice that the wavefunctions of interlayer Se ions are partly overlapped, the Pauli exclusion principle makes the two electrons in different Se-4p_z orbitals tend to have an antiparallel spin arrangement. As a result, the symmetric paths, i.e., the (θ_1, θ_1) and (θ_2, θ_2) paths, prefer the interlayer AFM order, while the asymmetric path (θ_1, θ_2) prefers the FM order. Considering that the interlayer SSE is greatly weakened by the vdW gap, the intralayer coupling has higher priority in meeting the Goodenough–Kanamori rule. The spin arrangement in Se···Se bond is forced to be parallel in the asymmetric path, which conflicts the Pauli exclusion principle. As a result, the overall ef-

fect of SSE coupling more likely to form the interlayer AFM order.

Considering the arrangement of interlayer Se ions, they are staggered in the AB- and A′B-stacking orders but are head-to-head in the AA′-stacking order. According to the SSE mechanism, the interlayer coupling in the AA′-stacking should be strongly antiferromagnetic. In Fig. 4(a), this is consistent with the DFT+U results but is contrary to the DFT results. The interlayer exchange in the AA′-stacking is ferromagnetic. Only considering the SSE mechanism can hardly explain this conflict. Notice that the major difference between DFT and DFT+U calculations lies in the bandgap opening in the FM bilayers, the DE mechanism mediated by conduction electrons can give a reasonable explanation. As schematically plotted in Fig. 4(d), the interlayer electrons hopping makes the DE prefer the FM order due to lower kinetic energy rather than the interlayer AFM order. The strength of DE directly relies on the density of carriers in bilayer VSe_2. For the AA′-stacking in DFT framework, the head-to-head Se-4p_z orbitals cause an extraordinarily strong interlayer hybridization and a high DOS at Fermi level, such that the interlayer DE makes the AA′-stacking are strong FM. On the whole, the interlayer magnetic coupling can be properly explained by the competition between the SSE and DE mechanisms.

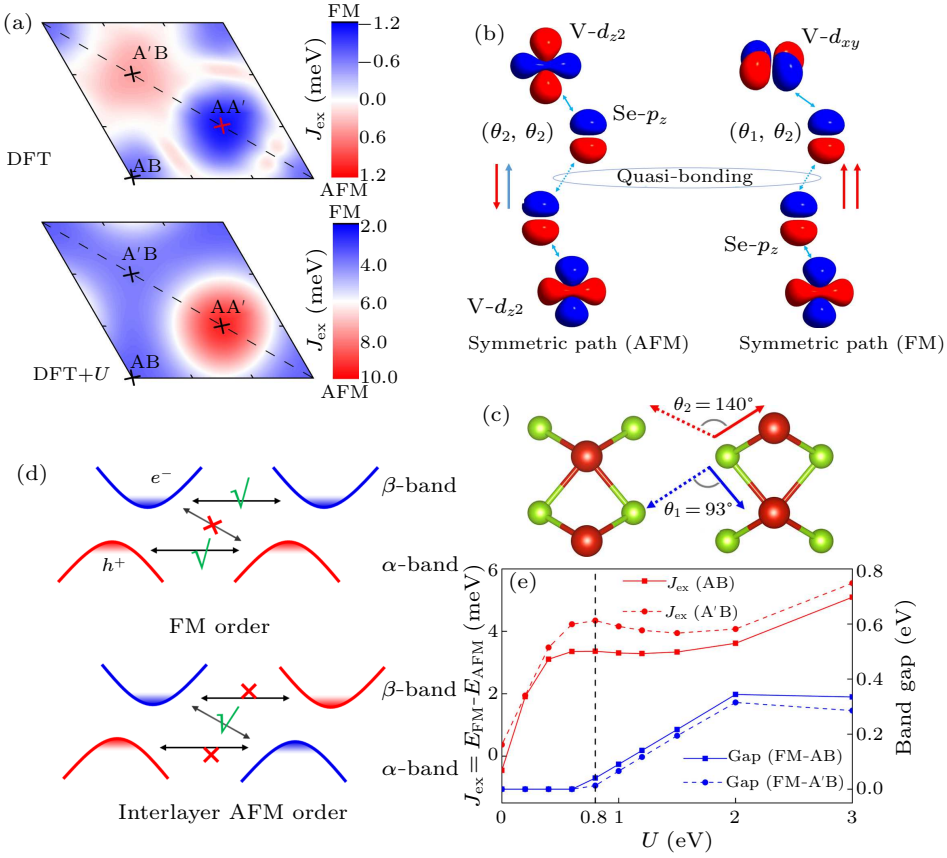

Fig. 4. (a) The landscape of the interlayer exchange energy without and with considering the Hubbard U correction. (b) Schematic of the interlayer SSE interaction. (c) The calculated V–Se···Se bond angles. (d) The interlayer DE interaction. (e) The change of interlayer exchange energy and band gaps with the increasing on-site Hubbard U parameter.

To further validate this competitive mechanism, we plot the interlayer exchange energy J_{ex} as a function of U in Fig. 4(e). When $U = 0$, the FM bilayer VSe_2 is metallic and the J_{ex} is close to zero, suggesting that the DE and the SSE are similar in strength, which makes the interlayer coupling be FM for the AB-stacking but be AFM for the A′B-stacking. When U increasing from 0 to 0.8 eV, the strength of DE decreases with the reduction of DOS at E_F. As a result, the J_{ex} monotonically increases in this range. Notice that a bandgap is opened in bilayer VSe_2 when $U = 0.8$ eV, also in which the increase of J_{ex} stops. This suggests that the most important role of Hubbard U correction is suppressing the DE coupling in bilayer VSe_2. Although the U parameter can also strengthen the interlayer SSE in some degree by increasing electronic interactions, the effect should be limited when U is not too large, because the interlayer SSEs are dominated by the low-localized interlayer Se-4p_z orbitals. In the literature, an effective U with a value of 1.16 eV is recommended,[22] which opens the bandgap and makes both AB- and A′B-stackings have the in-

terlayer AFM order. In the region of $U \in [0.8, 2.0]$ eV, the change of interlayer exchange energy is little, suggesting that the difference between the DFT+U and DFT results is mainly caused by the suppressing of DE.

We also calculated other possible magnetic orders, with their total energies much higher than the values of the FM order and interlayer AFM order. Furthermore, the Monte Carlo (MC) simulations were performed using the parameters obtained by our DFT+U calculations to estimate the Curie temperature. We find that the interlayer coupling plays an important role in the magnetism of magnetic multilayers, even though it is very weak in energy. These results can be found in the Supplementary Material.

To couple the stacking orders with different magnetic orders, one can use carrier doping to re-introduce the DE in bilayer VSe_2. Figure 5(a) shows the map of exchange energy J_{ex} as functions of the carrier density and the U parameter. A moderate hole doping in the magnitude of $10^{13}\,cm^{-2}$ is enough to change the bilayers from the interlayer AFM order to FM order, whereas doping electrons can only slightly reduce the J_{ex}. This difference can be understood by the distribution of additional charges after doping, as shown in Fig. 5(c). For the hole doping, a part of the carriers is distributed in the interlayer Se-4p_z orbital, which can help to strengthen the interlayer exchange. For the electron doping, few additional carriers are distributed in the interlayer region, such that its effect is greatly limited.

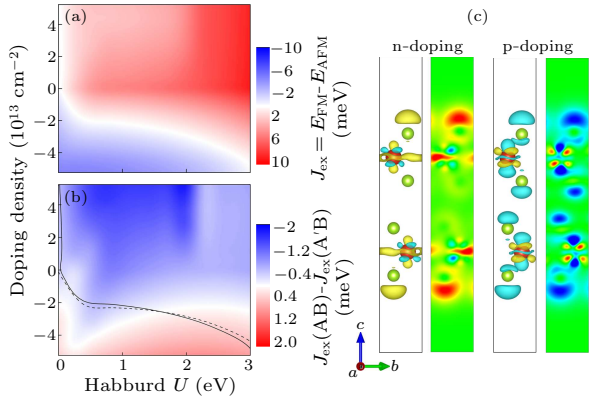

Fig. 5. (a) The exchange energy of AB-stacking as a function of doping density and Habbard U. (b) The difference of J_{ex} between AB- and A′B-stacking, where the solid and dashed lines represent $J_{ex} = 0$ for AB- and A′B-stackings, respectively. (c) The distribution of additional charges after electron and hole doping, where the contour surface is set as $10^{-4}\,e/Å^3$.

Since the J_{ex} is similar for the AB- and A′B-stackings, we only plotted the J_{ex} for AB-stacking in Fig. 5(a). Instead, we plot the difference of J_{ex} between AB- and A′B-stackings in Fig. 5(b). The solid and dashed lines represent the critical condition of AFM-to-FM transition for the AB- and A′B-stackings, respectively. A hole doping within $5 \times 10^{13}\,cm^{-2}$ can be used to couple the stacking orders with different interlayer magnetic orders. The required gate voltage can be estimated by a simple capacitor model:

$$V = \frac{Q}{C} = \frac{Q}{\varepsilon A/t} = \frac{e\sigma t}{\varepsilon_0 \varepsilon_r},$$

where e is the electron charge, σ is the doping density, t is the thickness of the dielectric layer, ε_0 and ε_r represent the vacuum and relative permittivity, respectively. Using the same parameters with a previous report (5 nm HfO_2, $\varepsilon_r = 25$),[34] the required voltage to control the interlayer magnetism is estimated to be ∼1.8 V.

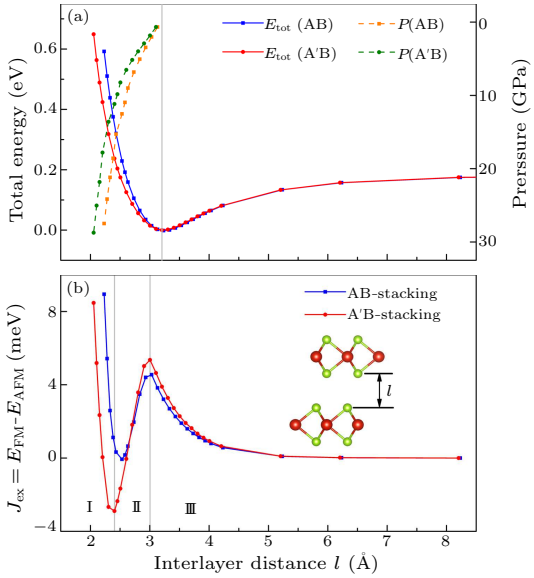

Fig. 6. (a) The total energy and pressure as a function of interlayer distance d. (b) The interlayer exchange energy U is set to 1 eV.

As the pressure-controlled interlayer magnetism in bilayer CrI_3 has been achieved by recent experiments,[8,9] we have also explored this possibility in bilayer VSe_2. The vertical pressure in bilayer VSe_2 can be written as $P = S^{-1} \times dE_{tot}/dl$, where S is the surface area, E_{tot} is the total energy and l is the interlayer distance. Figure 6(a) shows the total energy as a function of interlayer distance l. We find that there is a very tiny difference between the equilibrium distance of AB-stacking is imperceptibly larger than the one of A′B-stacking, on the value of 0.03 Å. Figure 6(b) shows the exchange energy as a function of interlayer distance, the interlayer magnetism of A′B-stacking is more sensitive to l than the one of AB-stacking. Interestingly, different from the Bethe–Slater–Curve-like behavior reported in bilayer $CrSe_2$ that only a single inflection point is observed,[18] the l–J_{ex} curves of bilayer VSe_2 have double inflection points. This difference is closely relevant to the semiconductor-to-metal transition in bilayer VSe_2. According to the inflection points, we can divide the curves into three regions, as marked in Fig. 6(b). In the region I, the wavefunctions

of interlayer Se-4p_z orbitals are highly overlapped, the strong Pauli repulsion makes the bilayers prefer the interlayer AFM order. In the region Ⅱ, the Pauli repulsion is weakened due to the increase of interlayer distance, whereas the bilayers are still metallic, such that the DE coupling can make the bilayers prefer the FM order. In region Ⅲ, as the interlayer hopping being further weakened, a bandgap is opened and the DE is fully suppressed. The SSE mechanism makes the bilayers prefer the interlayer AFM order.

In conclusion, based on first-principles calculations, we have studied the coupling between stacking orders and magnetic orders in bilayer H-VSe_2. We find that there are two stable stacking orders, AB-stacking and A′B-stacking. The interlayer Se-4p_z orbitals play a crucial role in the magnetic-order-dependent band splitting and interlayer exchange coupling. We have demonstrated that the interlayer magnetism is determined by the competition between the interlayer super-superexchange and the double exchange. Hole doping can significantly modulate the interlayer double exchange, therefore it can be used to control the AFM-to-FM transition in the bilayers and to lock the stacking modes with the magnetic orders. Our work gives a further understanding of the interlayer magnetism in TMDCs bilayers, and it may provide certain guidelines for the study of magnetic multilayers and heterostructures.

References

[1] Woomer A H, Druffel D L, Sundberg J D, Pawlik J T and Warren S C 2019 *J. Am. Chem. Soc.* **141** 10300
[2] Zhao Y D, Qiao J S, Yu P, Hu Z X, Lin Z Y, Lau S P, Liu Z, Ji W and Chai Y 2016 *Adv. Mater.* **28** 2399
[3] Jiang P H, Wang C, Chen D C, Zhong Z C, Yuan Z, Lu Z Y and Ji W 2019 *Phys. Rev. B* **99** 144401
[4] Sivadas N, Okamoto S, Xu X, Fennie C J and Xiao D 2018 *Nano Lett.* **18** 7658
[5] Gmitra M, Kochan D, Hogl P and Fabian J 2016 *Phys. Rev. B* **93** 155104
[6] Zhou W Z, Chen J Y, Yang Z X, Liu J W and Ouyang F P 2019 *Phys. Rev. B* **99** 075160
[7] Huang B, Clark G, Navarro-Moratalla E, Klein D R, Cheng R, Seyler K L, Zhong D, Schmidgall E, McGuire M A, Cobden D H, Yao W, Xiao D, Jarillo-Herrero P and Xu X D 2017 *Nature* **546** 270
[8] Zhou X Y, Wang C, Zhou L W, Pan Y H, Lu Z Y, Wan X G, Wang X Q and Ji W 2020 *Phys. Rev. B* **102** 020402
[9] Li T X, Jiang S W, Sivadas N, Wang Z F, Xu Y, Weber D, Goldberger J E, Watanabe K, Taniguchi T, Fennie C J, Mak K F and Shan J 2019 *Nat. Mater.* **18** 1303
[10] Song T C, Fei Z Y, Yankowitz M, Lin Z, Jiang Q N, Hwangbo K, Zhang Q, Sun B S, Taniguchi T, Watanabe K, McGuire M A, Graf D, Cao T, Chu J H, Cobden D H, Dean C R, Xiao D and Xu X D 2019 *Nat. Mater.* **18** 1298
[11] Gong C, Li L, Li Z L, Ji H W, Stern A, Xia Y, Cao T, Bao W, Wang C Z, Wang Y A, Qiu Z Q, Cava R J, Louie S G, Xia J and Zhang X 2017 *Nature* **546** 265
[12] Deng Y J, Yu Y J, Song Y C, Zhang J Z, Wang N Z, Sun Z Y, Yi Y F, Wu Y Z, Wu S W, Zhu J Y, Wang J, Chen X H and Zhang Y B 2018 *Nature* **563** 94
[13] Bonilla M, Kolekar S, Ma Y J, Diaz H C, Kalappattil V, Das R, Eggers T, Gutierrez H R, Phan M H and Batzill M 2018 *Nat. Nanotechnol.* **13** 289
[14] O'Hara D J, Zhu T C, Trout A H, Ahmed A S, Luo Y K, Lee C H, Brenner M R, Rajan S, Gupta J A, McComb D W and Kawakami R K 2018 *Nano Lett.* **18** 3125
[15] Hirahara T, Eremeev S V, Shirasawa T, Okuyama Y, Kubo T, Nakanishi R, Akiyama R, Takayama A, Hajiri T, Ideta S, Matsunami M, Sumida K, Miyamoto K, Takagi Y, Tanaka K, Okuda T, Yokoyama T, Kimura S, Hasegawa S and Chulkov E V 2017 *Nano Lett.* **17** 3493
[16] Tang Q K, Liu C Y, Zhang B B and Jie W Q 2018 *J. Solid State Chem.* **262** 53
[17] Gonzalez-Arraga L A, Lado J L, Guinea F and San-Jose P 2017 *Phys. Rev. Lett.* **119** 107201
[18] Wang X Q and Wu Z G 2017 *Phys. Chem. Chem. Phys.* **19** 2148
[19] Spiecker E, Schmid A K, Minor A M, Dahmen U, Hollensteiner S and Jager W 2006 *Phys. Rev. Lett.* **96** 086401
[20] Pan H 2014 *J. Phys. Chem. C* **118** 13248
[21] Tong W Y and Duan C G 2017 *npj Quantum Mater.* **2** 47
[22] Gong S J, Gong C, Sun Y Y, Tong W Y, Duan C G, Chu J H and Zhang X 2018 *Proc. Natl. Acad. Sci. USA* **115** 8511
[23] Kresse G and Furthmüller J 1996 *Phys. Rev. B* **54** 11169
[24] Perdew J P, Burke K and Ernzerhof M 1996 *Phys. Rev. Lett.* **77** 3865
[25] Blöchl P E 1994 *Phys. Rev. B* **50** 17953
[26] Bucko T, Hafner J, Lebegue S and Angyan J G 2010 *J. Phys. Chem. A* **114** 11814
[27] Dudarev S L, Botton G A, Savrasov S Y, Humphreys C J and Sutton A P 1998 *Phys. Rev. B* **57** 1505
[28] Esters M, Hennig R G and Johnson D C 2017 *Phys. Rev. B* **96** 235147
[29] Kasai H, Tolborg K, Sist M, Zhang J W, Hathwar V R, Filso M O, Cenedese S, Sugimoto K, Overgaard J, Nishibori E and Iversen B B 2018 *Nat. Mater.* **17** 249
[30] Zhao G M 2000 *Phys. Rev. B* **62** 11639
[31] Schlottmann P 2003 *Phys. Rev. B* **67** 174419
[32] Anderson P W 1950 *Phys. Rev.* **79** 350
[33] Goodenough J B 1955 *Phys. Rev.* **100** 564
[34] Zhang C X, Santosh K C, Nie Y F, Liang C P, Vandenberghe W G, Longo R C, Zheng Y P, Kong F T, Hong S, Wallace R M and Cho K 2016 *ACS Nano* **10** 7370

Supplementary Material: Coupling stacking orders with interlayer magnetism in bilayer H-VSe_2

Aolin Li(李奥林)[1], Wenzhe Zhou(周文哲)[1], Jiangling Pan(潘江陵)[2], Qinglin Xia(夏庆林)[2], Mengqiu Long(龙孟秋)[2,3], Fangping Ouyang(欧阳方平)[1,2,3**]

[1]*State Key Laboratory of Powder Metallurgy, and Powder Metallurgy Research Institute, Central South University, Changsha 410083, China*

[2]*School of Physics and Electronics, and Hunan Key Laboratory for Super-Microstructure and Ultrafast Process, Central South University, Changsha 410083, China*

[3]*School of Physics and Technology, Xinjiang University, Urumqi 830046, China*

** Corresponding author. Email: oyfp@csu.edu.cn

I. The phonon spectrum for bilayer VSe_2

To check the dynamical stability for AB- and A′B-stacking, the phonon dispersion relations are calculated and shown in Fig. S1, both the two stacking orders have not imaginary frequencies and are dynamical stable. The phonon spectrums for different interlayer magnetic orders and stacking orders have very little difference. Although the Hubbard U correction changes the frequencies of the optical branch in some degree, it has little influence on the acoustic branch and therefore does not affect the stability.

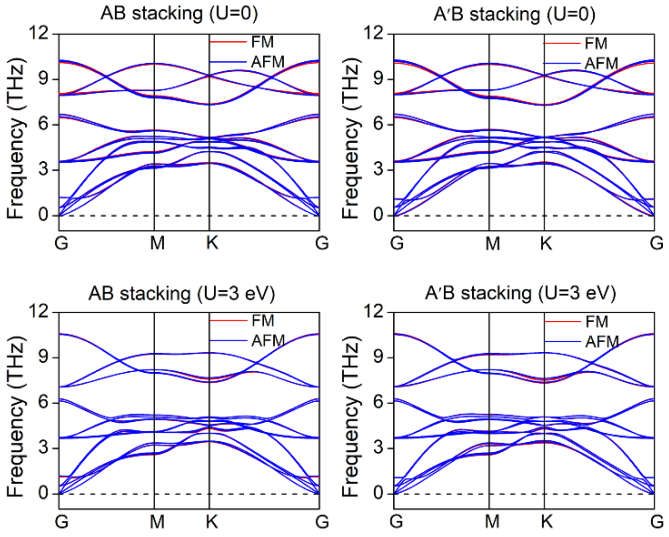

Fig. S1 The phonon dispersion relations for bilayer H-VSe_2.

II. Non-spin-polarized calculations for monolayer VSe_2

We show that a single band acrosses the Fermi level for the monolayer VSe_2 when spin-polarization is not considered in the DFT calculation. As shown in Fig. S2, the single band is mainly contributed by the V-3dz^2 orbital, and the Se-4p_z orbitals only have a very small contribution.

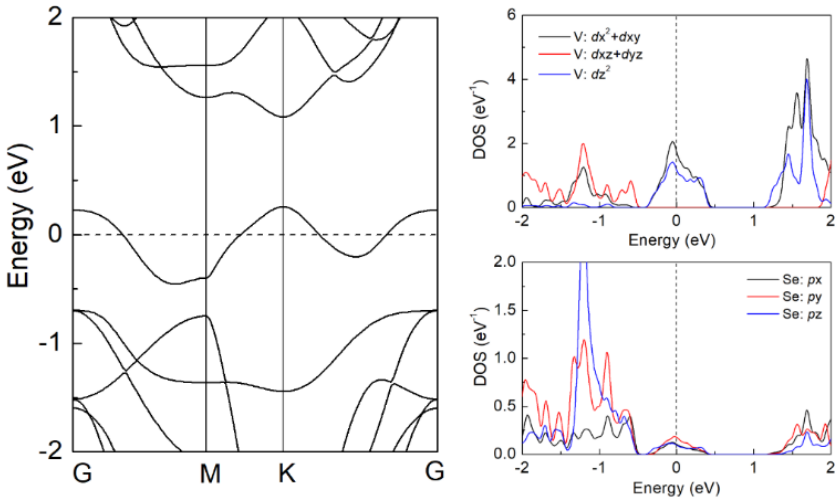

Fig. S2. The band structure and PDOS of monolayer H-VSe_2 without considering spin-polarization. The Fermi level is set as 0 eV.

III. Effects of Hubbard U and Spin-Orbit Coupling

We investigated the electronic structure of the monolayer VSe_2 under Hubbard U correction, as shown in Fig. S3. When the effective U parameter is not larger than ~2 eV, both the bandgap and the spin splitting energy (between the α- and β-band) go bigger with the increase of U. When the effective U parameter is larger than 2 eV, the α(β)-band is no longer the highest occupied (lowest unoccupied) band, and the bandgap changes little if U continue to increase.

The band structure of bilayer VSe_2 is shown in Fig. S4, which shows similar behavior under increasing U parameter. Noteworthy, the band splitting caused by the interlayer hopping in the FM bilayers is almost unaffected by the U parameter. This indicates the band splitting in the FM bilayers is dominantly by the interlayer Se ions rather than the V ions.

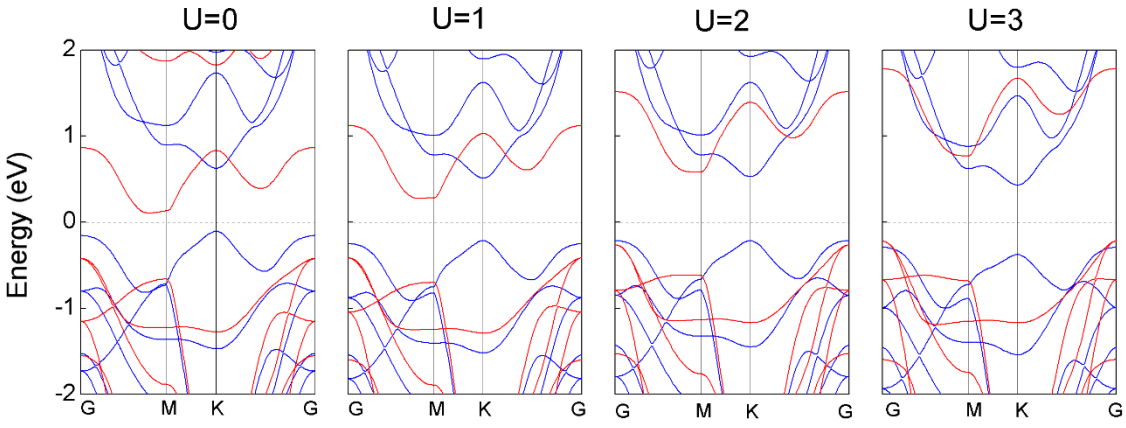

Fig. S3. The band structure for monolayer H-VSe_2 with different U, blue (red) line represents the spin up (down) component.

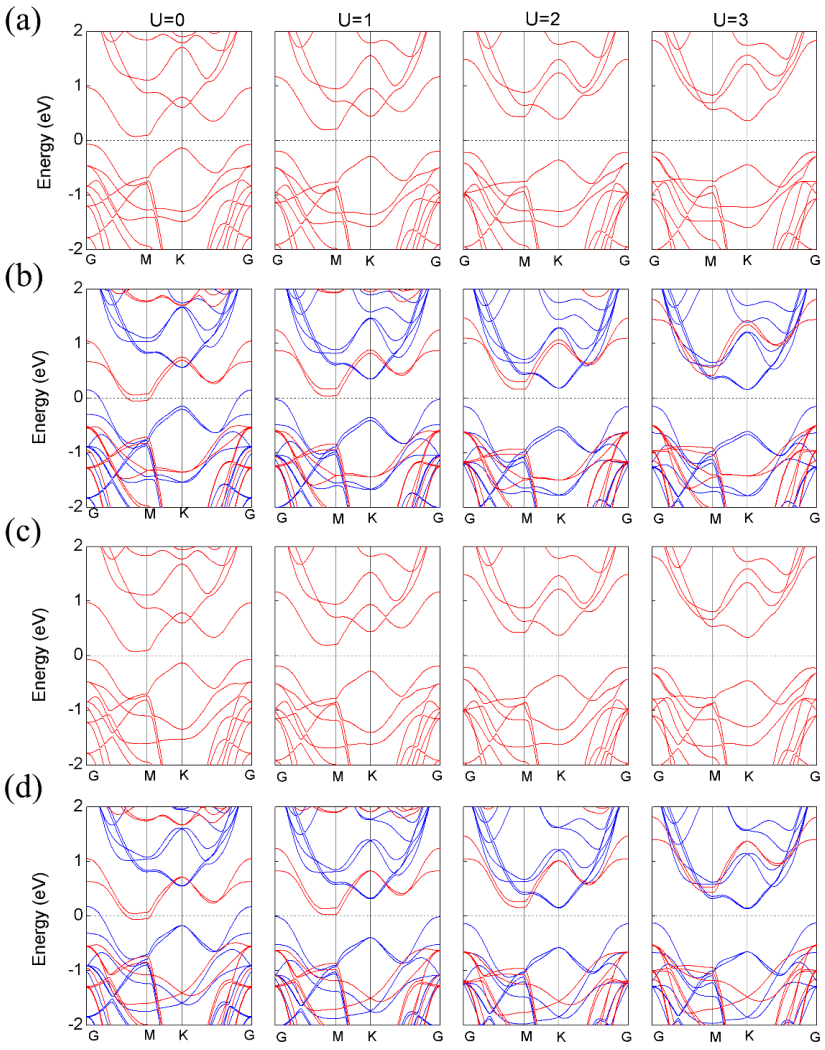

Fig. S4. The band structures for bilayer H-VSe_2 with different U, blue (red) line represents the spin up (down) band structure. (a) AFM AB-stacking; (b) FM AB-stacking; (c) AFM A′B-stacking; (d) FM A′B-stacking.

For checking the effect of spin-orbit coupling (SOC), we have performed DFT+SOC calculations. The calculated total energies are listed in Table S1, although considering SOC changes the total energy of the system, the energy difference between FM and AFM orders almost keep unchanged. Therefore, the effect of SOC has been neglected in this work.

Table S1 The total energy (eV) of bilayer H-VSe_2 calculated by different methods, U=1.0 eV.

	AB (FM)	AB (AFM)	A′B (FM)	A′B (AFM)
DFT	-37.3105	-37.3102	-37.3116	-37.3117
DFT+U	-35.2235	-35.2267	-35.2218	-35.2256
DFT+SOC	-37.3998	-37.3994	-37.4010	-37.4010
DFT+U+SOC	-35.3145	-35.3177	-35.3129	-35.3167

IV. Magnetic orders

We have considered two intralayer magnetic orders and five interlayer magnetic orders for VSe_2, as shown in Fig. S5. The corresponding total energies for these configurations are listed in Table S2. The monolayer VSe_2 with FM order is the most energy-favored, which consistent with the literature. For the bilayer, the energies of the FM order and the interlayer AFM order (AFM1) are much less than the values of other magnetic orders.

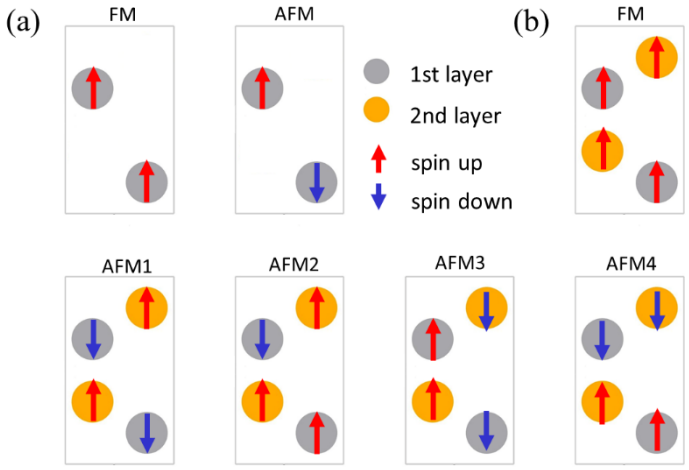

Fig. S5 Magnetic orders for VSe_2 monolayer (a) and AB-stacking bilayer (b). For simplicity, only V ions are plotted.

Table S2 Total energy (meV) for monolayer VSe_2 and AB-stacking bilayer VSe_2. The total energy of the (monolayer/bilayer) FM order is set as zero. In the bilayers, the configurations with the same intralayer magnetic order have very close total energy, suggesting very weak interlayer coupling in bilayer VSe_2.

		Monolayer		Bilayer				
U = 0 eV	Magnetic order	FM	AFM	FM	AFM1	AFM2	AFM3	AFM4
	Energy	0	151.82	0	0.35	135.93	276.31	276.13
U = 1 eV	Magnetic order	FM	AFM	FM	AFM1	AFM2	AFM3	AFM4
	Energy	0	220.23	0	-6.72	204.22	414.27	413.76

We use the Heisenberg model including the nearest-neighbor (NN) intralayer (J_1) and interlayer (J_2) exchange interactions to describe the magnetic interactions in this system. The spin Hamiltonian can be written as

$$\hat{H} = -J_1 \sum_{\langle ij \rangle} \left(\vec{S}_i \cdot \vec{S}_j + \vec{S}'_i \cdot \vec{S}'_j \right) - J_2 \sum_{\langle ij \rangle} \vec{S}_i \cdot \vec{S}'_j$$

where the summation $\langle ij \rangle$ runs over all of the NN Cr sites, $\vec{S}_i$ and $\vec{S}'_i$ represents the spin in the 1st and 2nd layer at site i, respectively. Here we adopt S = 3/2 for V ion.

The relative energies per unit cell for the bilayer H-VSe_2 can be written as:

$$E_{FM} = E_0 - 12J_1S^2 - 6J_2S^2$$

$$E_{AFM1} = E_0 - 12J_1S^2 + 6J_2S^2$$
$$E_{AFM2} = E_0 - 4J_1S^2$$

Where E_0 represents the total energy without magnetic couplings. Using the values in Table S2, we derived J_1 = 11.53 meV and J_2 = -0.25 meV, corresponding to the FM intralayer and AFM interlayer magnetic coupling, respectively. This suggests the ground state of bilayer H-VSe_2 is the A-type AFM order, in agreement with previous works [1, 2].

We used Monte Carlo (MC) simulations with the Wolff algorithm to estimate the Curie temperature [3]. To demonstrate the effect of interlayer coupling, three different sets of parameters were used in the MC simulations. In Fig. S5(a), the estimated Neel temperature of bilayer H-VSe_2 is about 523 K. Assuming that the interlayer magnetic coupling was reversed by charge doping (Fig. S5(b)), the bilayer H-VSe_2 will have a ferromagnetic ground state. Fig. S5(c) shows the results without interlayer coupling, the Curie temperature reduces about 26 K compared with Fig. S5(a) and (b). These results suggest the interlayer coupling plays an important role in the magnetism of magnetic multilayers, even though it is very weak in energy.

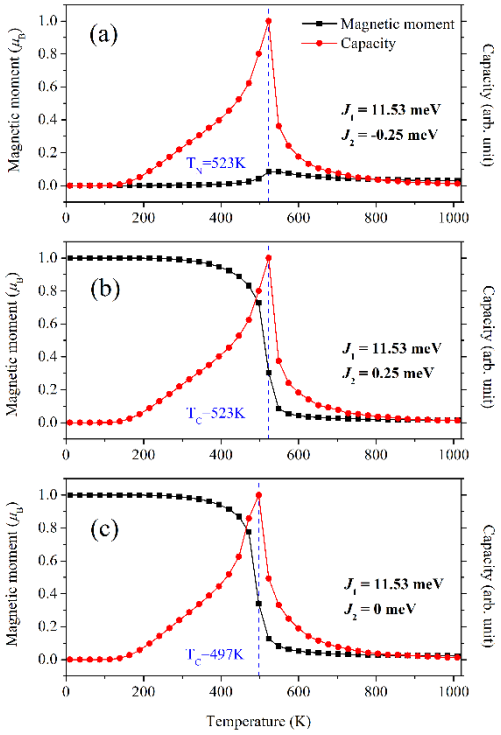

Fig. S6 Variation of the total magnetic moment per V ion and thermal capacity with respect to the temperature.

References

[1] Esters M, Hennig R G and Johnson D C 2017 *Phys. Rev. B* 96, 235147

[2] Gong S J, Gong C, Sun Y Y, Tong W Y, Duan C G, Chu J H and Zhang X 2018 *Proc. Natl. Acad. Sci. USA* 115, 8511-8516

[3] Liu L, Ren X, Xie J H, Cheng B, Liu W K, An T Y, Qin H W and Hu J F 2019 *Appl. Surf. Sci.* 480, 300-307